NONLINEAR EVOLUTION EQUATIONS IN QCD*

Anna M. Staśto

Physics Department, Brookhaven National Laboratory
Upton, NY 11973, USA†
and
H. Niewodniczański Institute of Nuclear Physics
Polish Academy of Sciences
Radzikowskiego 152, 31-342 Kraków, Poland

(Received November 9, 2004)

These lectures are an introduction to the phenomenon of partonic saturation and nonlinear evolution equations in Quantum Chromodynamics. After short introduction to linear evolution, the problem of unitarity bound and parton saturation are discussed. The nonlinear Balitsky–Kovchegov evolution equation in the high energy limit is introduced and the progress in understanding the properties of its solution is reviewed. We discuss saturation scale, geometrical scaling and lack of infrared diffusion. Finally, we give a brief summary of current theoretical developments which go beyond the Balitsky–Kovchegov equation.

PACS numbers: 12.38.Bx

1. Introduction

One of the most intriguing problems in Quantum Chromodynamics is the growth of the cross sections for hadronic interactions with energy. Imagine the two particles are scattering at very high energy, Fig. 1. While energy grows, there is an increased probability for emission of soft particles. In the case of QED one would have to consider diagram of the type shown on the left hand plot in Fig. 1. While in QCD one also has these diagrams, there are additional diagrams of the type on the right plot in Fig. 1. Since gluons carry color charge and couple to each other, the increase of energy will cause a fast growth of the gluon density and consequently of the cross section. This increase will lead to the formation of the dense, colored medium

* Presented at the XLIV Cracow School of Theoretical Physics, Zakopane, Poland, May 28–June 6, 2004.
† Permanent address.

at very high energies. This type of medium can be obtained at high energies in deep inelastic lepton–nucleon scattering, hadron–hadron, nucleus–nucleus or even virtual photon scattering.

Fig. 1. Scattering of two hadronic probes at high energy. Left: QED-type diagrams; right: diagrams with gluon self-interactions.

In perturbative QCD the growth of the gluon density in the limit of high energy is governed by the BFKL Pomeron [1]. The solution to this equation gives a very strong, power-like growth of the gluon density and also of the resulting cross section

$$f(x) \ \sim \ x^{-\lambda} ,$$

where x is Bjorken variable (fraction of longitudinal momentum of the target) and $\lambda = ((4 \ln 2N_c)/\pi)\alpha_{\rm s}$ is the intercept of the perturbative Pomeron in the leading logarithmic (LLx, $\ln 1/x \gg 1$) approximation. In the pioneering paper [2], Gribov, Levin and Ryskin proposed that the gluon recombination might be important at high energies and it would decrease the growth of the parton density. This is called *perturbative partonic saturation*. In [2], a new nonlinear evolution equation in double leading logarithmic approximation (DLLA, $\ln 1/x \ln Q^2 \gg 1$) for the gluon density has been proposed which apart from gluon production takes into account also recombination effects

$$Q^2 \frac{\partial^2 xG(x,Q^2)}{\partial \ln 1/x \partial Q^2} = \frac{\alpha_{\rm s} N_c}{\pi} xG(x,Q^2) - \frac{4\alpha_{\rm s}^2 N_c}{3C_{\rm F} R^2} \frac{1}{Q^2} \left[xG(x,Q^2) \right]^2 . \quad (1)$$

Note negative sign in front of the nonlinear term which is responsible for the gluon recombination. The strong growth generated by the linear DLLA term is damped whenever gluon density $xG(x,Q^2)$ becomes large, of the order $1/\alpha_{\rm s}$.

Partonic saturation is also very important in the context of the unitarity bound. It is well known that the hadronic cross sections should obey the Froissart bound [3] which is derived from the general assumptions on the analyticity and unitarity of the scattering amplitude. According to this bound the total cross section cannot grow faster than the logarithm squared of the energy

$$\sigma_{\rm tot} = \frac{\pi}{m_\pi^2} (\ln s)^2 \,, \tag{2}$$

with m_π being the scale which characterizes the range of the strong force. It is believed, that the parton saturation could be a mechanism which leads to the unitarization of the cross section at high energies. Unfortunately the problem is rather complex since parton saturation is a purely perturbative mechanism while the Froissart bound has been derived from general principles and refers to the QCD as a complete theory of strong interactions together with nonperturbative effects. After the GLR equation (1) was proposed, there has been an increasing activity in developing the theory which would describe saturation at high energies. The effective theory for a high density partonic systems at small x is Color Glass Condensate [4] with the resulting JIMWLK evolution equations [5], see also [6]. Another approach has been developed by Balitsky [7] where he constructed an infinite hierarchy of coupled equations for correlators of Wilson lines. In the mean field approximation the first equation of this theory decouples and is equivalent to the Kovchegov equation [8] derived independently in the dipole approach [9]. It is a nonlinear equation for the dipole scattering amplitude which is valid in the leading $\log 1/x$ approximation. The Balitsky–Kovchegov equation is perhaps the best known equation which includes saturation effects and which can be relatively simply solved, at least numerically. These lectures are meant to introduce the reader into the phenomenon of partonic saturation and the concept of nonlinear evolution on the example of Balitsky–Kovchegov (BK) equation. We start with a brief recap of the linear evolution in QCD. We recall the Froissart bound and the necessary conditions which lead to its derivation. Then the Balitsky–Kovchegov equation is introduced and the properties of its solution are investigated such as infrared diffusion, saturation scale and geometrical scaling. We also present an analysis of this equation in more general case of 4 dimensions, which takes into account spatial distribution of the dipoles in impact parameter space. We finish by a short outlook and discussion of recent theoretical developments in this field.

2. DIS kinematics and variables

In the following we will mainly concentrate on the deep inelastic scattering process of lepton off the hadron or nucleus. For completeness we recall first basic kinematics of DIS, see Fig. 2. The total energy squared of the electron–nucleon system is $s_{(eN)} = (p+k)^2$ whereas that of photon–nucleon $s_{\gamma^* N} = (p+q)^2$. Negative photon virtuality is denoted by $q^2 = (k-k')^2 = -Q^2 < 0$ and the Bjorken variable $x = \frac{Q^2}{2p\cdot q} = \frac{Q^2}{Q^2 + s_{(\gamma^* N)}}$. The high energy regime that we are working in, is defined equivalently as

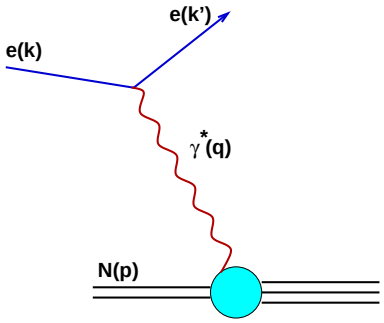

Fig. 2. Deep inelastic scattering process of electron on the hadronic target.

$$\begin{aligned} s_{(\gamma^* N)} &\longrightarrow \infty\,, \\ x &= \frac{Q^2}{Q^2 + s_{(\gamma^* N)}} \simeq \frac{Q^2}{s_{(\gamma^* N)}} \longrightarrow 0\,, \\ Y &= \ln 1/x \longrightarrow \infty. \end{aligned} \tag{3}$$

3. Linear evolution equations in QCD

Let us consider a scattering of photon with virtuality Q^2 off a hadron at center of mass energy $\sqrt{s}$. The photon virtuality defines a resolution scale $\lambda \sim 1/\sqrt{Q^2}$ with which one probes a partonic structure of the hadron, see left hand plot in Fig. 3. At given resolution $t = \ln Q^2/Q_0^2$ photon probes a density of partons $q(x,t)$ with fraction of a hadron momentum $x = Q^2/s$. By increasing Q^2 one increases also the resolution, so the density of quarks is larger: $q(x,t) + \delta q(x,t)$, see the right-hand plot in Fig. 3. This process can be described as a following linear evolution equation for density

$$\frac{\partial q(x,t)}{\partial t} = \frac{\alpha_s(t)}{2\pi} \int_x^1 \frac{dy}{y} P_{qq}\left(\frac{x}{y}\right) q(y,t)\,. \tag{4}$$

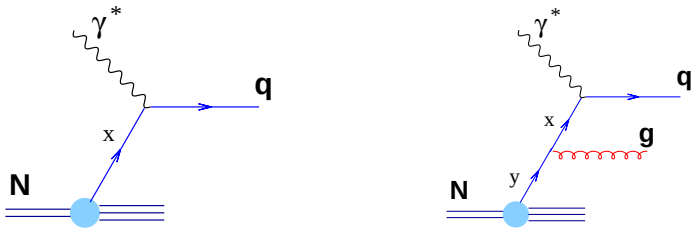

Fig. 3. Left: photon with virtuality Q^2 probes quark with a longitudinal momentum fraction x. Right: the virtuality (resolution) is increased so the density of quarks also grows.

The splitting function $P_{qq}(z = x/y)$ describes a probability of finding quark inside the quark with fraction $z = x/y$ of the parent quark momentum. This is one of the set of the well known DGLAP evolution equations [10]. For the DGLAP equations to be complete, apart from the quark density $q(x,t)$ one has to include the gluon density $g(x,t)$ which is coupled to q. The evolution of the gluon density is shown in diagrams in Fig. 4. The full set of singlet DGLAP evolution equations reads as follows

$$\frac{\partial}{\partial t}\begin{bmatrix} \sum(x,t) \\ g(x,t) \end{bmatrix} = \frac{\alpha_{\rm s}(t)}{2\pi}\begin{bmatrix} P_{qq} & 2N_f P_{qg} \\ P_{gq} & P_{gg} \end{bmatrix} \overset{x}{\otimes} \begin{bmatrix} \sum(x,t) \\ g(x,t) \end{bmatrix},$$

where $\sum(x,t) = \sum\limits_i [q_i(x,t) + \bar{q}_i(x,t)]$ is the singlet quark density.

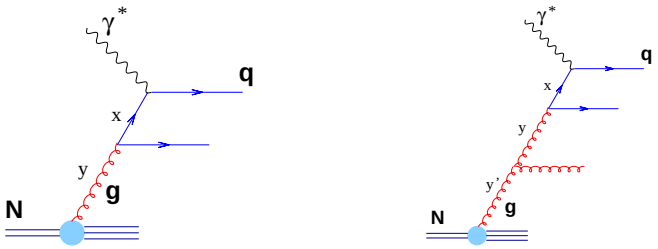

Fig. 4. Additional set of diagrams present in the DGLAP evolution.

An approach which is alternative to DGLAP [1] is to consider fixed virtuality of the probe and to increase the energy s (or alternatively rapidity Y) see Fig. 5. This leads to the BFKL equation

$$\frac{\partial G(Y,t)}{\partial Y} = \frac{\alpha_{\rm s} N_c}{\pi} \int dt' \mathcal{K}(t,t') G(Y,t')\,, \tag{5}$$

which is an evolution equation in rapidity Y. Quantity $\mathcal{K}(t,t')$ is Lipatov kernel which describes probability of branching of the gluon with virtuality t' into virtuality t. The function $G(Y,t)$ is called unintegrated gluon density and it is related to $g(x,t)$ from (4)

$$g(x,t) = \int^t dt'\, G(x,t')\,.$$

Both $\mathcal{K}$ and P_{ij} have perturbative expansions in $\alpha_{\rm s}$. These both quantities have a finite number of common terms in the expansion. The solution to the BFKL equation has the following form, see for example [11]

$$G(x) \sim x^{-\lambda_{\rm P}}\,, \qquad \lambda_{\rm P} = 4\ln 2 \frac{N_c \alpha_{\rm s}}{\pi}\,. \tag{6}$$

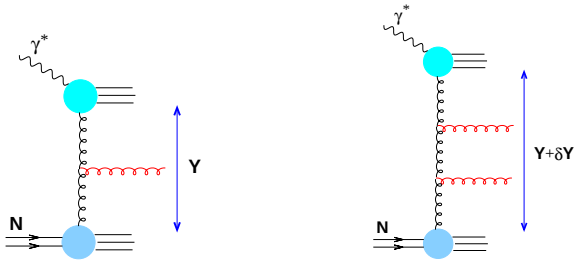

Fig. 5. Evolution in the BFKL framework: virtualities of probes are fixed and energy is increased.

This solution exhibits very strong rise with $1/x$ (and correspondingly with energy $s = Q^2/x$) which is in contradiction with Froissart bound [3].

4. Froissart bound

In this section we recall the basic assumptions that go into the derivation of the Froissart bound [3]. This bound applies for the total cross section for scattering of two hadrons and reads as follows

$$\sigma_{\rm tot} \leq \frac{\pi}{m_\pi^2} (\ln s)^2 \,. \tag{7}$$

Its derivation is based on the two assumptions: unitarity of partial amplitudes and the finite length of the strong interaction. The first condition says that scattering matrix S has to be unitary

$$S^\dagger S = S S^\dagger = 1 \,. \tag{8}$$

If we consider set of particle states $|m\rangle$ they have to satisfy completeness relation

$$\sum_m |m\rangle\langle m| = 1 \,. \tag{9}$$

Then the probability that a given final state $|f\rangle$ comes from an initial state $|i\rangle$ is given by

$$P_{fi} = |\langle f|S|i\rangle|^2 \,. \tag{10}$$

The sum of these probabilities over initial states have to give 1 since a probability that a given final state comes from any initial state is 1

$$\sum_f P_{fi} = \langle i|S^\dagger S|i\rangle = 1 \,. \tag{11}$$

The latter equation gives condition for the S-matrix to be unitary (8).

A second important assumption is the one about the finite range of strong force. This means that there must be a certain mass scale present in the theory which will cut off the interaction

$$R \sim \frac{1}{m_\pi}\,. \tag{12}$$

This scale is entirely nonperturbative and cannot be computed from perturbative tools of QCD. By using these two assumptions together and the Mandelstam representation, the Froissart bound can be derived [3]. One has to stress that the Froissart bound applies for the complete QCD theory which includes both perturbative and non-perturbative parts. It is perhaps worthwhile mentioning that while one believes that Froissart bound should be valid for QCD, it is not clear that one can easily see it from the data. The structure function data for deep inelastic scattering at high photon virtualities exhibit rather strong rise with decreasing x, which is consistent with a power $x^{-\lambda}$ with $\lambda \simeq 0.35$, and no sign of the logarithmic dependence is seen, compare Fig. 6. Pinning down the saturation effects in the experimental data is a very nontrivial task. One problem with the structure function data is that it is a completely inclusive measurement. In particular structure function F_2 is averaged over the impact parameter of the $\gamma^* - p$ collision and it is known that saturation effects crucially depend on this variable. Therefore, saturation should be searched in more exclusive processes, for example like diffraction. For more information on the phenomenology of saturation see [12, 13] and references therein.

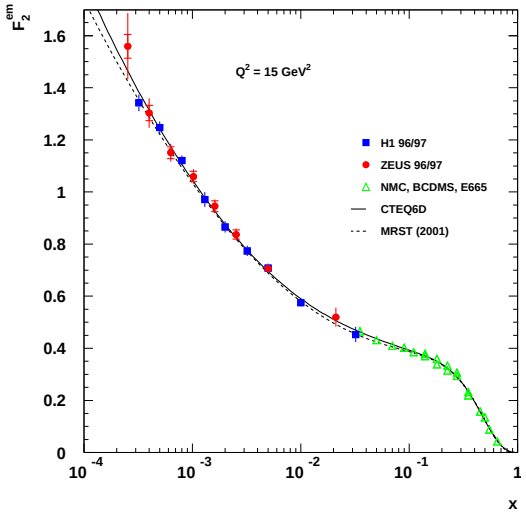

Fig. 6. F_2 structure function data from HERA collider and fixed target experiments.

5. Parton saturation and nonlinear evolution

Given the fact that the Froissart bound should be satisfied, a natural question arises: how one should modify the perturbative evolution in order to tame the growth of the cross section? One would like to identify the Feynman diagrams which are responsible for the gluon recombination and derive appropriate evolution equations which include these additional diagrams. As already stated in the introduction, the standard evolution equations lead to a strong rise of the parton density with energy. One can expect that when the density of partons becomes very large they will start to overlap. The schematic picture of the saturation phenomenon is shown in Fig. 7. The horizontal axis is the energy whereas the vertical one is the parton size defined by the inverse of the photon virtuality $r \sim 1/Q$, in the deep inelastic scattering process. The onset of saturation depends on energy but also on the parton size. The larger the size of the partons, the earlier they will fill up available area and start to re-interact. Further increase in the energy will not increase probed parton density. Therefore, apart from production diagrams one has to include additional diagrams which take into account gluon recombination. This leads to the modification of the evolution equation by term which is nonlinear in density. The first equation of this type was the GLR equation [2] already mentioned in the introduction

$$Q^2 \frac{\partial^2 xG(x,Q^2)}{\partial \ln 1/x \partial Q^2} = \frac{\alpha_{\rm s} N_c}{\pi} xG(x,Q^2) - \frac{4\alpha_{\rm s}^2 N_c}{3C_{\rm F} R^2} \frac{1}{Q^2} \left[xG(x,Q^2)\right]^2 . \qquad (13)$$

The first term on the right hand side is the usual DGLAP term in the double logarithmic approximation, $\ln 1/x \ln Q^2/\Lambda^2 \gg 1$, whereas the second, nonlinear term, is responsible for the gluon recombination. The nonlinear term is inversely proportional to the hadron area $\sim R^2$ and the scale $\sim Q^2$ at which the gluon density is being probed. The smaller the hadron area in

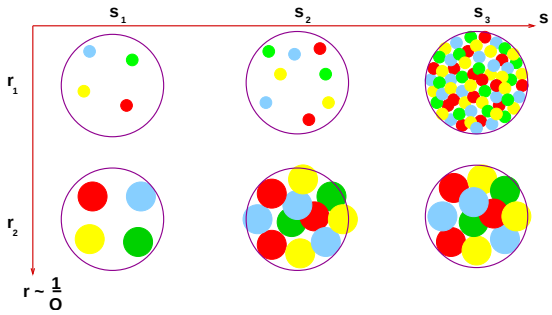

Fig. 7. Schematic view of parton saturation. Horizontal axis is energy squared s, the vertical axis is r, the parton size.

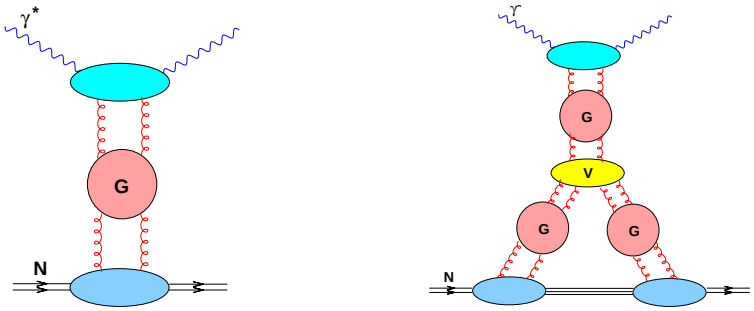

Fig. 8. Left: linear evolution, right: fan diagrams summed by the nonlinear GLR (13).

impact parameter the earlier the partons will fill it up and saturate. Scale Q^2 defines the parton size $r \sim 1/Q$: when it is small the saturation will be delayed to larger energies.

The GLR equation sums a particular set of diagrams, called *fan diagrams*, (illustrated on the right-hand plot in Fig. 8) within the double leading logarithmic approximation.

The nonlinear Balitsky–Kovchegov (BK) equation which is valid in the leading logarithmic $\ln 1/x$ approximation has been derived independently by Kovchegov [8] within the dipole formulation of high energy scattering and by Balitsky [7] from the operator product expansion for high energy scattering. More precisely, Balitsky's equations form an infinite hierarchy of coupled equations for correlators of Wilson lines, and only in the mean field approximation the first equation decouples and is equivalent to the equation derived by Kovchegov. An independent approach is that of Color Glass Condensate [4] in which the evolution is governed by the JIMWLK functional equation [5] equivalent to Balitsky hierarchy. In this lecture we will study the solution of the Balitsky–Kovchegov equation which is currently the simplest tool to describe the parton saturation phenomenon.

6. Multiple scattering in dipole picture

In this section we will follow the derivation of the BFKL [9] and BK [8] equations in the dipole picture. One starts with the heavy quark–antiquark pair, *onium*, see Fig. 9, which wave function in the momentum space is denoted by

$$\psi^{(0)}_{\alpha\beta}(k_1, z_1)\,,$$

where k_1 is the transverse momentum of the quark and $z_1 = (k_{1+})/(p_+)$ is the fraction of light cone momentum.

The dipole picture is formulated by going to transverse coordinate space

$$\psi^{(0)}_{\alpha\beta}(\boldsymbol{x}_0, \boldsymbol{x}_1, z_1) = \int \frac{d^2\boldsymbol{k}_1}{(2\pi)^2}\, e^{i\boldsymbol{x}_{01}\cdot\boldsymbol{k}_1} \psi^{(0)}_{\alpha\beta}(\boldsymbol{k}_1, z_1)\,,$$

$$\Phi^{(0)}(\boldsymbol{x}_0, \boldsymbol{x}_1, z_1) = \sum_{\alpha,\beta} |\psi^{(0)}_{\alpha\beta}(\boldsymbol{x}_0, \boldsymbol{x}_1, z_1)|^2 \,,$$

where now $\boldsymbol{x}_0, \boldsymbol{x}_1$ denote the positions of the quark and antiquark, end points of the *dipole*.

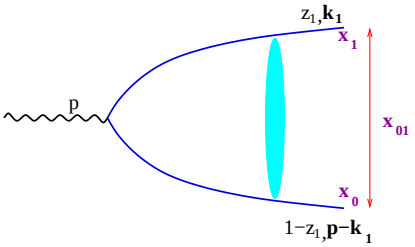

Fig. 9. Heavy quark–antiquark dipole onium.

Now one adds one soft gluon, Fig. 10, which means that its longitudinal momentum is much smaller than that of the original quark (antiquark) $z_2/z_1 \ll 1$.

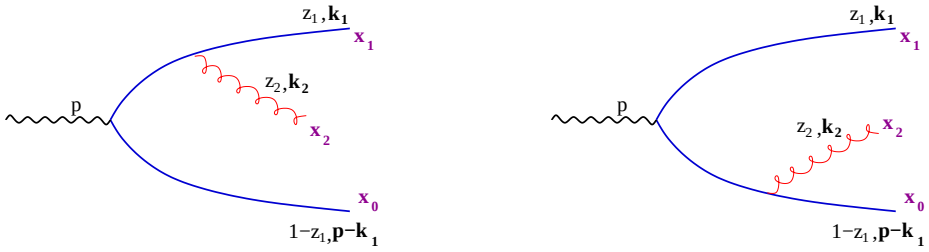

Fig. 10. Onium with additional one soft gluon.

The relation between one-gluon wave function $\Phi^{(1)}$ and wave function of the onium without any soft gluons is expressed as

$$\Phi^{(1)}(\boldsymbol{x}_0, \boldsymbol{x}_1, z_1) \;=\; \frac{\alpha_{\rm s} C_{\rm F}}{\pi^2} \int\limits_{z_0}^{z_1} \frac{dz_2}{z_2} \int d^2\boldsymbol{x}_2 \frac{\boldsymbol{x}_{01}^2}{\boldsymbol{x}_{20}^2 \boldsymbol{x}_{12}^2} \Phi^{(0)}(\boldsymbol{x}_0, \boldsymbol{x}_1, z_1) \,.$$

In the limit of large number of colors the gluon can be represented by a quark–antiquark pair, as in Fig. 11. The emission of one additional gluon is equivalent to the splitting of the original dipole $(0,1)$ into two dipoles $(0,2)$ and $(2,1)$ with probability of branching given by the measure

$$d^2\,\boldsymbol{x}_2 \frac{\boldsymbol{x}_{01}^2}{\boldsymbol{x}_{20}^2 \boldsymbol{x}_{12}^2} \,.$$

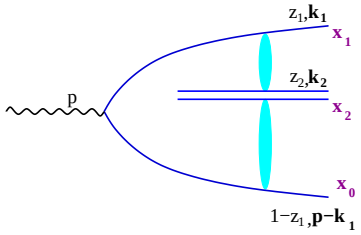

Fig. 11. Onium wave function which consists of two dipoles.

The process of emissions of subsequent soft dipoles can be repeated in the analogous way to obtain the wave function with arbitrary number of gluons $\Phi^{(n)}$, see Fig. 12. To describe this process, Mueller [9] introduced a generating functional for dipoles

$$Z(\boldsymbol{b}_{01}, \boldsymbol{x}_{01}, z_1, u)\,,$$

which satisfied normalization condition

$$Z(\boldsymbol{b}_{01}, \boldsymbol{x}_{01}, z_1, u = 1) = 1\,.$$

Performing functional differentiation of Z, the wave functions for arbitrary number of gluons can be obtained as follows

$$\begin{aligned}\Phi^{(n)}(\boldsymbol{x}_0, \boldsymbol{x}_1, \boldsymbol{x}_2, \ldots, \boldsymbol{x}_{n+1}) \;&=\; \Phi^{(0)} \frac{\delta}{\delta u(\boldsymbol{x}_2)} \frac{\delta}{\delta u(\boldsymbol{x}_3)} \ldots \\ &\quad \times \frac{\delta}{\delta u(\boldsymbol{x}_{n+1})} Z(\boldsymbol{x}_0, \boldsymbol{x}_1, z_1, u)|_{u=0}\,.\end{aligned}$$

$\Phi^{(n)}$ gives probability of finding n daughter dipoles which originate from parent quark–antiquark dipole $(0, 1)$. The daughter dipoles are produced in positions x_k with $k = 2, \ldots, n$. In the following, we also introduced another convenient notation with

$$\boldsymbol{x}_{01} \equiv \boldsymbol{x}_0 - \boldsymbol{x}_1\,,$$

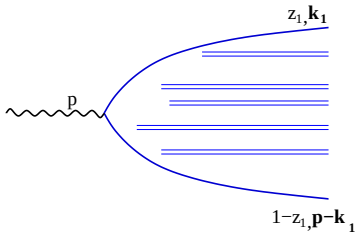

Fig. 12. Onium wave function with arbitrary number of dipoles.

being the transverse size of the dipole and

$$\boldsymbol{b}_{01} \equiv \frac{\boldsymbol{x}_0 + \boldsymbol{x}_1}{2}\,,$$

being the impact parameter (position) of this dipole.

By investigating the relation between wave functions with n and $n+1$ dipoles Mueller derived [9] the differential equation for the generating functional

$$\frac{dZ(\boldsymbol{b}_{01}, \boldsymbol{x}_{01}, y, u)}{dy} = \int \frac{d^2\boldsymbol{x}_2 \boldsymbol{x}_{01}^2}{\boldsymbol{x}_{20}^2 \boldsymbol{x}_{12}^2} \times \left[Z(\boldsymbol{b}_{01} + \frac{\boldsymbol{x}_{12}}{2}, \boldsymbol{x}_{20}, y, u)\, Z(\boldsymbol{b}_{01} - \frac{\boldsymbol{x}_{20}}{2}, \boldsymbol{x}_{12}, y, u) - Z(\boldsymbol{b}_{01}, \boldsymbol{x}_{01}, y, u) \right], \quad (14)$$

where the evolution variable is the rapidity $y = \ln 1/z_+$. From the above equation for the functional, one can obtain the evolution equation for the scattering amplitude of dipole on the target. First, one has to construct the number density for dipoles from generating functional

$$n_1(x_{01}, \boldsymbol{x}, \boldsymbol{b} - \boldsymbol{b}_0, Y) = \frac{\delta}{\delta u(\boldsymbol{b}, \boldsymbol{x})}\, Z(\boldsymbol{b}_{01}, \boldsymbol{x}_{01}, Y, u)|_{u=1}\,,$$

or in general the density for k dipoles

$$n_k = \prod_{i=1}^{k} \frac{\delta}{\delta u(\boldsymbol{b}_i, \boldsymbol{x}_i)}\, Z|_{u=1}\,. \quad (15)$$

The amplitude for scattering of one dipole on a target, see left plot in Fig. 13, can be then obtained by convoluting the dipole number density with the propagator of that dipole in the nucleus

$$N_1(\boldsymbol{x}_{01}, \boldsymbol{b}_{01}, Y) = \int d[\mathcal{P}_1] n_1\, \gamma_1\,, \quad (16)$$

where

- $d[\mathcal{P}]_1 = \frac{d^2\boldsymbol{x}_1}{2\pi x_i^2} d^2\boldsymbol{b}_1$ phase space measure;
- $\gamma \equiv \gamma(\boldsymbol{x}, \boldsymbol{b})$ propagator of single dipole in the nucleus.

By differentiating equation for generating functional and using relation (16) one can obtain the linear evolution equation for the dipole–target amplitude

$$\frac{dN_1(\boldsymbol{b}_{01}, \boldsymbol{x}_{01}, Y)}{dY} = \bar{\alpha}_{\rm s} \int \frac{d^2\boldsymbol{x}_2\, \boldsymbol{x}_{01}^2}{\boldsymbol{x}_{20}^2\, \boldsymbol{x}_{12}^2} \times \left[N_1(\boldsymbol{b}_{01} + \frac{\boldsymbol{x}_{12}}{2}, \boldsymbol{x}_{20}, Y) + N_1\left(\boldsymbol{b}_{01} - \frac{\boldsymbol{x}_{20}}{2}, \boldsymbol{x}_{12}, Y\right) - N_1\left(\boldsymbol{b}_{01}, \boldsymbol{x}_{01}, Y\right) \right]. \quad (17)$$

It has to be stressed, that only the contribution which comes from the *single scattering* of one dipole on the target has been included in the derivation. The above equation (17) is the dipole version of the BFKL equation in the transverse coordinate space derived in [9]. One can also generalize this equation by taking into account multiple scattering of many dipoles on the target, see right plot in Fig. 13. To this aim one takes the number density of k dipoles Eq. (15), and convolutes it with k propagators for these dipoles. The following expression for the amplitude is then obtained

$$N(\boldsymbol{x}_{01}, \boldsymbol{b}_{01}, Y) = \sum_{k=1}^{\infty} \int d[\mathcal{P}_k]\, n_k\, \gamma_1 \dots \gamma_k\,, \tag{18}$$

where now the measure is defined as

$$[\mathcal{P}]_k = \prod_{i=1}^{i=k} \frac{d^2\boldsymbol{x}_i}{2\pi x_i^2} d^2\boldsymbol{b}_i\,.$$

Again by differentiation of the equation for the generating functional Z one can obtain the evolution equation for the amplitude which takes into account multiple scatterings [8]

$$\begin{aligned}\frac{dN(\boldsymbol{b}_{01}, \boldsymbol{x}_{01}, Y)}{dY} &= \bar{\alpha}_{\rm s} \int \frac{d^2\boldsymbol{x}_2\, \boldsymbol{x}_{01}^2}{\boldsymbol{x}_{20}^2\, \boldsymbol{x}_{12}^2} \\ &\times \left[N\left(\boldsymbol{b}_{01} + \frac{\boldsymbol{x}_{12}}{2}, \boldsymbol{x}_{20}, Y\right) + N\left(\boldsymbol{b}_{01} - \frac{\boldsymbol{x}_{20}}{2}, \boldsymbol{x}_{12}, Y\right) - N(\boldsymbol{b}_{01}, \boldsymbol{x}_{01}, Y) \right. \\ &\left. - N\left(\boldsymbol{b}_{01} + \frac{\boldsymbol{x}_{12}}{2}, \boldsymbol{x}_{20}, Y\right) N\left(\boldsymbol{b}_{01} - \frac{\boldsymbol{x}_{20}}{2}, \boldsymbol{x}_{12}, Y\right) \right]. \end{aligned} \tag{19}$$

The characteristic feature of this equation is its nonlinearity. Thus in the dipole approach the multiple scattering of many dipoles in the onium wave function leads to nonlinear evolution equation for the amplitude. This has to be contrasted with the single scattering of one dipole which leads to the linear BFKL-type evolution equation. One has to stress that this multiple

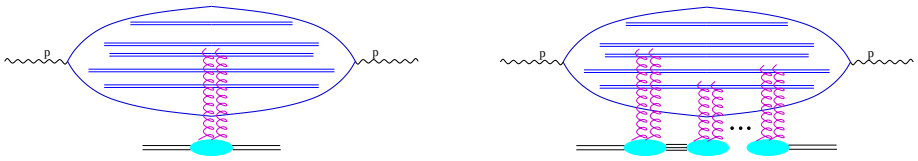

Fig. 13. Left: single dipole scattering which leads to linear BFKL evolution Eq. (17). Right: multiple dipole scattering which results in nonlinear Balitsky–Kovchegov evolution Eq. (19).

scattering is completely incoherent process: dipoles scatter independently of each other, there are no correlations. This is quite an important simplification which actually enables to arrive at one, relatively simple, closed evolution equation. These correlations are a subject of intensive scientific research and we will return to this problem at the end of this lecture.

7. Balitsky–Kovchegov equation at high energies

In the next sections we are going to study the solutions of the Balitsky–Kovchegov equation

$$\frac{dN(\boldsymbol{b}_{01},\boldsymbol{x}_{01},Y)}{dY} = \bar{\alpha}_{\rm s}\int \frac{d^2\boldsymbol{x}_2\,\boldsymbol{x}_{01}^2}{\boldsymbol{x}_{20}^2\,\boldsymbol{x}_{12}^2} \times\left[N\left(\boldsymbol{b}_{01}+\frac{\boldsymbol{x}_{12}}{2},\boldsymbol{x}_{20},Y\right)+N\left(\boldsymbol{b}_{01}-\frac{\boldsymbol{x}_{20}}{2},\boldsymbol{x}_{12},Y\right)-N(\boldsymbol{b}_{01},\boldsymbol{x}_{01},Y) - N\left(\boldsymbol{b}_{01}+\frac{\boldsymbol{x}_{12}}{2},\boldsymbol{x}_{20},Y\right)\,N\left(\boldsymbol{b}_{01}-\frac{\boldsymbol{x}_{20}}{2},\boldsymbol{x}_{12},Y\right)\right]. \tag{20}$$

Let us list the basic features of this equation

- It is an evolution equation in rapidity $Y=\ln 1/x$.
- One needs to specify the initial conditions $N^{(0)}(\boldsymbol{b}_{01},\boldsymbol{x}_{01},Y=0)$ which depend on the target of the specific process.
- This equation is valid in the leading logarithmic approximation in which the powers in $(\alpha_{\rm s}\ln 1/x)^n$ are being summed. In this approximation the strong coupling $\alpha_{\rm s}$ is fixed.
- $\boldsymbol{b}_{01}$ is the impact parameter whereas $\boldsymbol{x}_{01}$ size of the dipole, see Fig. 14. The whole problem involves $(4+1)$ variables: 4 degrees of freedom per dipole and 1 evolution variable.

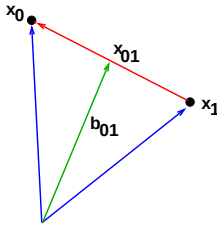

Fig. 14. Schematic representation of the dipole position in impact parameter space. $(\boldsymbol{x}_0,\boldsymbol{x}_1)$ denote end points of the dipole.

7.1. Toy model in (0+1) dimensions

In searching for solutions to Eq. (20) let us first observe this equation has two fixed points

$$\frac{dN(\boldsymbol{b}_{01}, \boldsymbol{x}_{01}, Y)}{dY} = 0\,,$$

which are

$$N = 0 \qquad \text{and} \qquad N = 1\,.$$

It is quite instructive to investigate first the toy model in (0+1) dimensions, that is when amplitude is only dependent on rapidity $N \equiv N(Y)$ and the kernel is simply some number. In this case the equation reduces to

$$\frac{dN}{dY} = \omega(N - N^2)\,,\ \omega > 0\,.$$

The above equation was first discussed by Verhulst in 1838 as a model for self-limiting population growth in biology. The solution to this equation can be easily found

$$N(Y) = \frac{e^{\omega Y}}{e^{\omega Y} + C^{-1}}\,, \qquad N^{(0)}(Y = 0) = C\,,$$

and is illustrated in Fig. 15. It is also called logistic curve. The crucial property of this solution is that it saturates for very large values of Y

$$\forall_{C \neq 0}\ N(Y) \overset{Y \to \infty}{\longrightarrow} 1\,,$$

in contrast to the solution of the linear equation which grows exponentially with increasing Y.

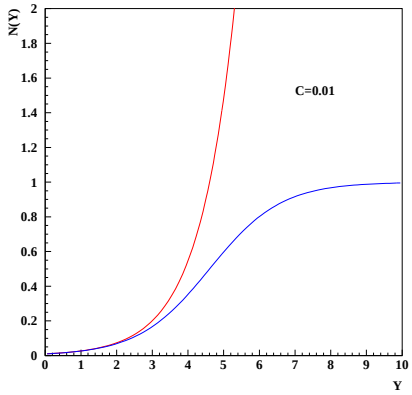

Fig. 15. Illustration of the solution to the Verhulst equation (saturated line) and the linear equation (exponentially increasing).

Thus the toy model teaches us that the fixed point $N = 0$ is an unstable one with respect to linear part of the evolution. On the other hand, point $N = 1$ is a fixed one. After sufficiently large interval of evolution in Y the solution will reach this point, starting from any initial condition (provided $N^{(0)}(Y = 0) \neq 0$).

8. Solution in (1+1) dimensions

Having briefly looked at toy model let us proceed to the full equation. As already stated it depends on $(4 + 1)$ variables which makes it very difficult to solve even numerically. The biggest complication is that variables $\boldsymbol{b}_{01}$ and $\boldsymbol{x}_{01}$ are entangled in the arguments of the functions N, see Eq.(20). However, let us observe that the kernel depends only on sizes $\boldsymbol{x}_{01}, \boldsymbol{x}_{20}, \boldsymbol{x}_{12}$. By assuming that the solution N has translational invariance

$$N(\boldsymbol{b}_{01}, \boldsymbol{x}_{01}, Y) \to N(|\boldsymbol{x}_{01}|, Y)\,,$$

the problem is reduced to $(1 + 1)$ dimensions with no dependence on impact parameter $\boldsymbol{b}_{01}$. Physically, this corresponds to scattering on infinite and uniform nucleus. BK equation in this approximation in $(1 + 1)$ dimensions has been extensively studied numerically [14–17] and analytically [18–20].

In Fig. 16 we illustrated rapidity dependence of $N(Y, r = |\boldsymbol{x}_{01}|)$ for two, fixed values of r and compared with the solution to the linear equation. We observe that the solution to the BK equation has qualitatively the same features as the toy model. For a given r the solution of the nonlinear equation tends to unity, whereas the linear solution exponentially increases.

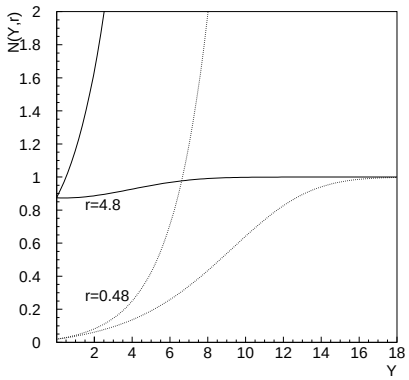

Fig. 16. Rapidity dependence of the solution to $(1 + 1)$ dimensional Balitsky–Kovchegov equation (saturated lines) for two, fixed values of the dipole size r as compared to the solution of the linear BFKL equation (exponentially increasing).

Also the system saturates earlier, that is for smaller values of Y when the dipole size is larger. To understand this feature better let us now look at the solution as a function of dipole size r for given, fixed values of Y. The characteristic feature is that the amplitude saturates to 1 for smaller dipoles as rapidity increases. In the following, see Fig. 17, we also studied the dependence on different initial conditions. In Fig. 17 several initial conditions has been shown, all of them had different normalization and also with different type of behavior for large values of r ($N(r) \to 1$ or $N(r) \to 0$ as $r \to \infty$). In all cases the solution shows a universal shape, with $N = 0$ being an unstable fixed point and $N = 1$ being the stable one.

8.1. Saturation scale

The solution shown in Fig. 17 can be divided into three regions: region where the amplitude is small and the nonlinear corrections are negligible, region where the amplitude $N \sim 1$ and the transition region between the two. This boundary can be characterized by introducing saturation scale $Q_{\mathrm{s}}(Y)$

$$r < \frac{1}{Q_{\mathrm{s}}(Y)} \;\to\; N \ll 1\,,$$
$$r > \frac{1}{Q_{\mathrm{s}}(Y)} \;\to\; N \sim 1\,.$$

From the solution to the Balitsky–Kovchegov equation one can extract this saturation scale. It turns out that its leading rapidity dependence is exponential

$$Q_{\mathrm{s}}(Y) = Q_0 \exp(\bar{\alpha}_s\, \lambda\, Y)\, Y^{-\beta}\,, \qquad \lambda \simeq 2.4\,,$$

with some subleading corrections, see [19, 21].

The qualitative properties of the Balitsky–Kovchegov equation are (very roughly) similar to the properties of the dipole cross section from the Golec–Biernat and Wusthoff saturation model [13]. There, the following form of the dipole cross section has been postulated

$$\sigma(Y, r) \equiv \int d^2\boldsymbol{b}\, N(\boldsymbol{b}, r, Y) = \sigma_0 \left[1 - \exp\left(-\frac{r^2 Q_{\mathrm{s}}^2(Y)}{4}\right)\right], \qquad (21)$$

with the rapidity-dependent saturation scale: $Q_{\mathrm{s}}^2(Y) = e^{0.28(Y - Y_0)}$. The constant normalization σ_0 has been adjusted to fit the experimental data: $\sigma = 23\mathrm{mb}$. In the regime where dipoles are smaller than the inverse of the

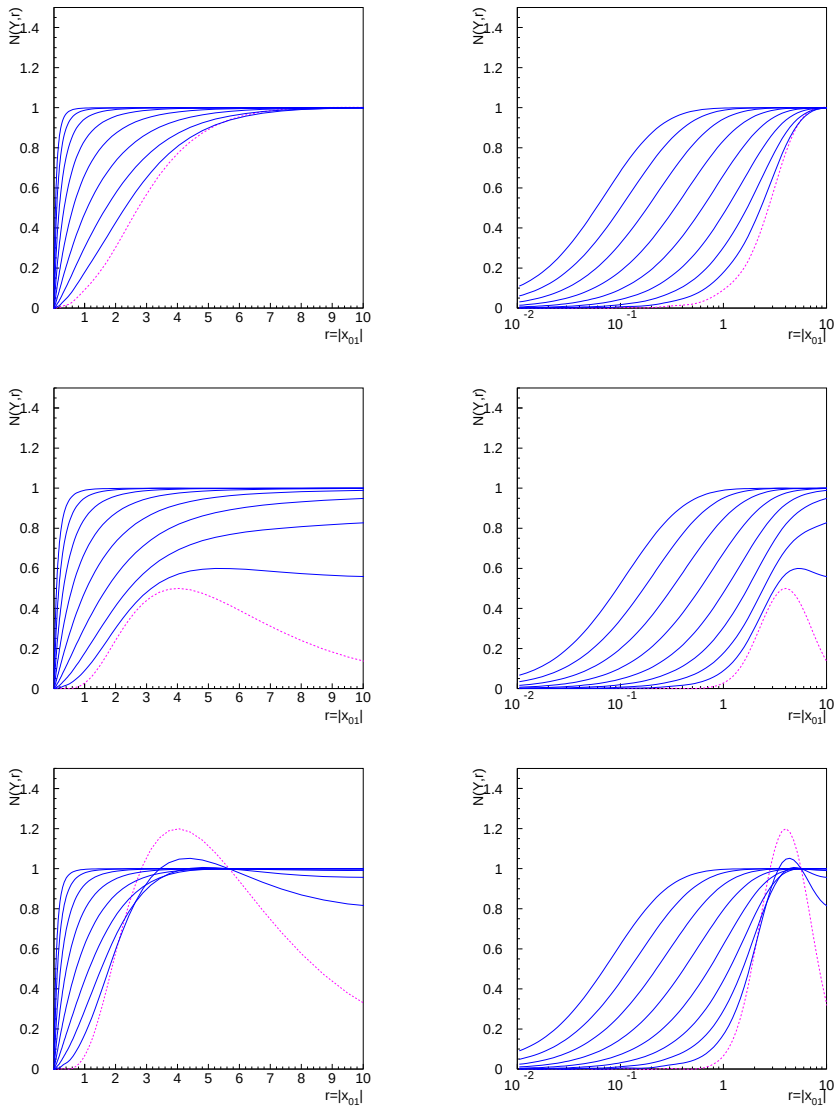

Fig. 17. Dipole size dependence of the solution to the $(1+1)$ dimensional Balitsky–Kovchegov equation for different values of rapidity Y. From up to down: different initial conditions; left: linear scale; right: logarithmic scale. Dashed line denotes the initial distribution at $Y = 0$. Solid lines from right to left are for increasing values of rapidity.

characteristic saturation scale $r < 1/Q_{\rm s}(Y)$ the cross section is small and proportional to

$$\frac{\sigma(r,Y)}{\sigma_0} \simeq \frac{r^2 Q_{\rm s}^2(Y)}{4}\,,$$

in accord with the color transparency. When we consider large dipoles such that $r > 1/Q_{\rm s}(Y)$ the cross section saturates to σ_0 so that

$$\frac{\sigma(r,Y)}{\sigma_0} \simeq 1\,,$$

becomes independent of both r and Y.

8.2. Geometrical scaling and traveling waves

While investigating the solution as a function of the dipole size r one observes that the solution reaches universal shape independently of the initial condition. When evaluated at different values of rapidity Y the solution looks similar, with only difference that it is being shifted towards smaller values of dipole size. This property is known as *geometrical scaling* and it was first postulated to be observed in the experimental data at HERA electron–proton collider [22], see also [23]. Mathematically, geometrical scaling means that the solution to the BK equation depends only on one combined variable

$$rQ_{\rm s}(Y)\,,$$

instead of r and Y separately, *i.e.*

$$N(r,Y) \equiv N(rQ_{\rm s}(Y))\,.$$

When written in terms of logarithms of variables and using the rapidity dependence of the saturation scale $Q_{\rm s}(Y) \simeq Q_0 \exp(\bar{\alpha}_{\rm s}\lambda_{\rm s}Y)$

$$\ln r + \ln Q_{\rm s}(Y) = \ln r + \bar{\alpha}_{\rm s}\lambda_{\rm s}Y\,.$$

If we interpret $\ln r$ as a spatial coordinate and Y as time, then geometrical scaling simply means that the solution is a wave front moving with a constant velocity $\bar{\alpha}_{\rm s}\lambda_{\rm s}$, see [19]. It has been also described as a soliton wave in [14]. The scaling property is also present in the Golec–Biernat and Wusthoff saturation model (21).

The transition between the dilute and saturated regimes can be illustrated in the following diagram, see Fig. 18. The critical line dividing dense and dilute regions is the saturation scale. The higher the rapidity the denser the system gets and partons start to re-interact. Also the saturation occurs earlier if the size of the partons is bigger.

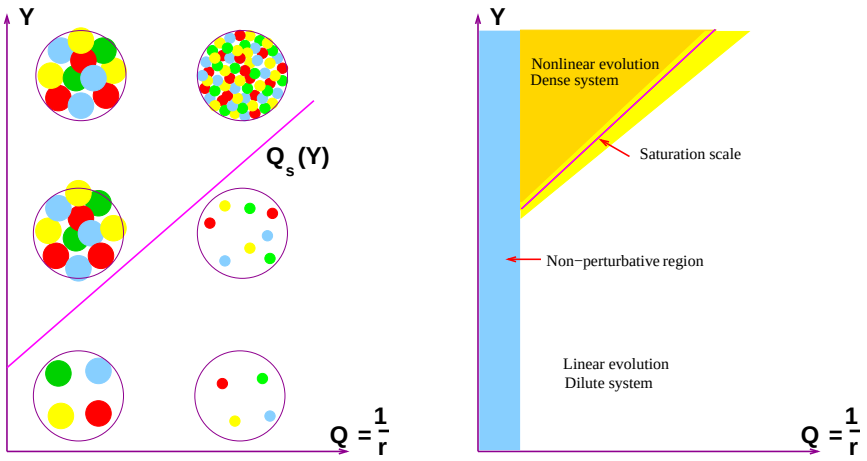

Fig. 18. Schematic representation of dilute and saturated regions in the kinematic space (Q, Y).

9. Diffusion properties of the BK equation

Up to now we have looked at the solutions of the BK equation directly in the coordinate space as it has been originally formulated. By performing Fourier transform and going into momentum space

$$\phi(k,Y) := \int_0^\infty \frac{dr}{r} J_0(k\,r)\, N(r,Y)\,,$$

one can obtain quite compact form of this equation

$$\frac{d\phi(k,Y)}{dY} = \bar{\alpha}_{\rm s} \int \frac{dk'}{k'}\, \mathcal{K}(k,k')\, \phi(k',Y) - \bar{\alpha}_{\rm s}\phi^2(k,Y)\,, \tag{22}$$

in $(1+1)$ dimensions. In Eq. (22) the integral operator $\mathcal{K}(k,k')$ is the usual BFKL kernel in momentum space.

The solution to the linear part of the equation is very well known and in the saddle point approximation it has the following form

$$k\phi(k,Y) = \frac{1}{\sqrt{\pi\bar{\alpha}_{\rm s}\chi''(0)Y}}\, \exp(\bar{\alpha}_{\rm s}\chi(0)Y)\, \exp\left(-\frac{\ln^2(k^2/k_0^2)}{2\bar{\alpha}_{\rm s}\chi''(0)Y}\right). \tag{23}$$

First exponential is responsible for the fast increase of the gluon density with rapidity where $\chi(0) = 4\ln 2$ is the famous BFKL intercept. Second exponential causes the diffusion of the momenta into ultraviolet and infrared regions. It is well known that the BFKL equation has this property of

strong diffusion, it can be interpreted as a random walk in the $\ln k$ space of transverse momenta. The rapidity (energy) plays here the role of the time. In left plot of Fig. 19 we have illustrated the numerical solution to the BFKL as a function of transverse momentum for fixed values of rapidity Y. The Gaussian shape expected from (23) is clearly visible and its width is increased when rapidity grows. This is potentially a problem since one is starting from a perturbative calculation at a fixed, large scale k_0, but after some evolution in rapidity, nonperturbative regime of $\Lambda_{\mathrm{QCD}} \sim k \ll k_0$ is reached. The situation is quite different in the case of the nonlinear Balitsky–Kovchegov equation, which is illustrated by solid lines on right plot of Fig. 19. Clearly, the diffusion into infrared is very suppressed in the case of the solution to the BK equation. The peak of the distribution moves away from the initial value k_0 to larger values of k with increasing Y. It turns out that one can define saturation scale as a position of this maximum

$$Q_{\mathrm{s}}(Y) \equiv k_{\max}(Y)\,.$$

This property of suppressed diffusion can be also visualized in a different way by looking at the following renormalized distribution

$$\Psi(k,Y) = \frac{k\phi(k,Y)}{k_{\max}(Y)\phi(k_{\max}(Y),Y)}\,. \tag{24}$$

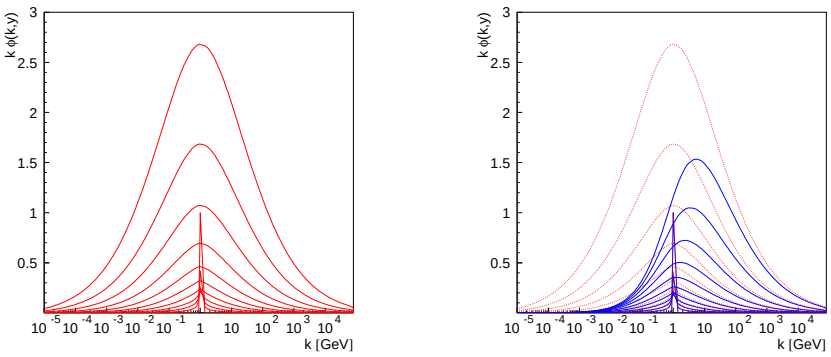

Fig. 19. Left: solution to the BFKL equation in the momentum space as a function of momentum k for various fixed values of rapidity $Y = 1, \ldots, 10$; right: the same but both BFKL (dashed) and BK (solid) solutions are showed.

On right plot of Fig. 20 we have shown the contour plot in (k, Y) space of this distribution for the case of the linear BFKL equation. Contour lines denote constant values of the renormalized distribution $\Psi(k, Y)$. The diffusive character of the solution to linear BFKL equation is clearly visible.

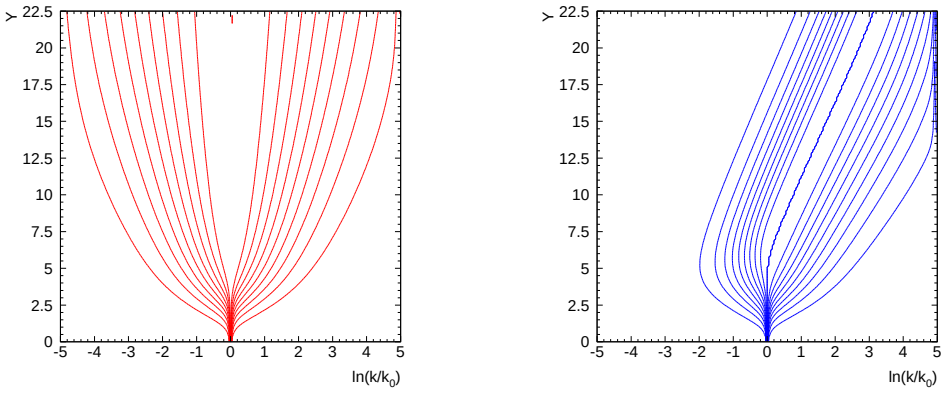

Fig. 20. Contour plots of the renormalized distribution $\Psi(k, Y)$ in the case of the linear BFKL solution and the nonlinear BK solution.

On the right plot of Fig. 20 we show the contour plot of the solution to the nonlinear BK equation. We see that the contour lines are shifted towards the higher values of transverse momenta[1]. We can also identify a line in (k, Y) space which divides a region where there is still a diffusion (to the right) and where there is no diffusion, and the contour lines are parallel to each other. These straight parallel lines mean that the solution is scaling there since one can parameterize them by $\xi = \ln k/k_0 - \lambda Y + \xi_0$ and the solution is only dependent on ξ. The critical line defines the saturation scale that was introduced in the previous paragraphs. It turns out that, the nonlinear BK equation can be approximated as a diffusion equation with the absorptive boundary which is (or close to) critical line defined by the saturation scale $Q_{\mathrm{s}}(Y)$ [21]. One can get very precise evaluation of the rapidity dependence of the saturation scale using this approximation. Recently, there has been quite substantial development in the understanding of the solutions to the $(1 + 1)$ dimensional BK equation. In series of important papers [19] it was proved, that BK equation can be approximated as a diffusion equation with nonlinear term. It is then equivalent to the Fisher–Kolmogorov–Petrovsky–Piscounov (FKPP) equation [24]

$$\partial_t u(t, x) = \partial_x^2(t, x) + u(t, x)[1 - u(t, x)]\,, \tag{25}$$

where the change of variables from $(Y, \ln k)$ to (t, x) has been performed with simultaneous identification of $\phi \to u$. FKPP equation has been previously studied in many fields of physics, for a review see for example [25], and

[1] A distortion of the contours at the highest values of k is unphysical and is caused by cutoffs in numerical calculation.

its solutions are very well understood. In particular it is well known that the FKPP equation has traveling wave solution for large times (which are equivalent to large energies) which is just a property of geometrical scaling.

9.1. BK equation with running coupling

As already stated, the BK equation has been derived within the LLx approximation in which the coupling constant is fixed. It is very well known fact, that NLLx effects in the BFKL formalism are very important [26]. At NLLx order the coupling runs and it is well known that the linear BFKL equation becomes very unstable in that case. To be precise, the linear evolution becomes very sensitive to the details of the running coupling regularization. This effect is illustrated in Fig. 21 where we show the solution $k\phi^{\mathrm{BFKL}}(k,Y)$ in the case of the running coupling as a function of the transverse momentum for increasing values of Y. One sees that the position of the maximum changes rapidly from initial condition $k = k_0$, to very low values of momenta, where they are determined by the regularization of the running coupling, $k \simeq k_{\mathrm{reg}} \ll k_0$. We have introduced the running coupling into the BK equation in the following way

$$\frac{d\phi(k,Y)}{dY} = \bar{\alpha}_{\mathrm{s}}(k) \int \frac{dk'}{k'} \mathcal{K}(k,k')\, \phi(k',Y) - \bar{\alpha}_{\mathrm{s}}(k)\phi^2(k,Y)\,. \tag{26}$$

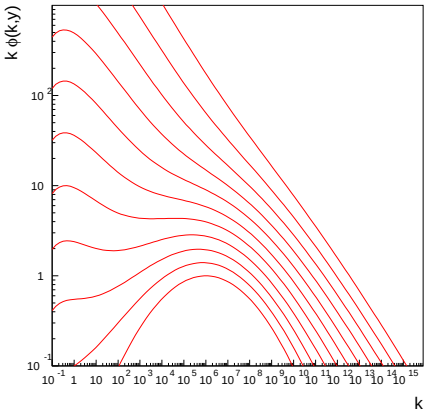

Fig. 21. Solution to the BFKL equation with running coupling.

The solution to the above equation is illustrated in Fig. 22 where it has been superimposed onto the solution of the linear BFKL equation. It is clear that the solution is much more stable than in the linear case, the maximum of

the distribution is not shifted to the infrared, rather it moves towards higher values of transverse momenta as rapidity increases. The reason for this is that the nonlinear term strongly damps the diffusion into the infrared regime. The saturation scale $Q_{\rm s}(Y)$ provides a natural cutoff for the low momenta and so no dependence on the regularization of the running coupling is seen (see for example [17, 27–29].

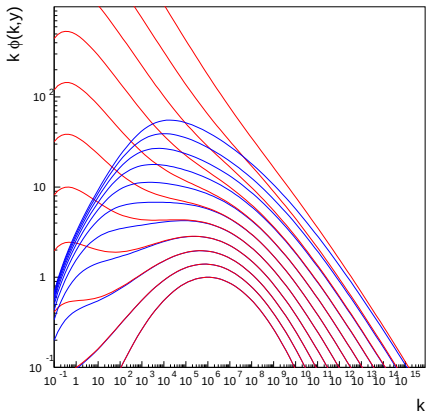

Fig. 22. Solution to the BK equation (as compared to BFKL) with running coupling.

One might ask whether the geometrical scaling is still preserved in the presence of the additional scale $\Lambda_{\rm QCD}$ which is introduced by the running coupling. It turns out that it still holds, though the saturation scale has different rapidity dependence (see [17, 21, 29–31] and also [2]

$$Q_{\rm s}(Y) = \Lambda_{\rm QCD} \exp\left(\sqrt{\frac{12c}{\beta_0}(Y - Y_0) + \ln^2 \frac{Q_0}{\Lambda_{\rm QCD}}}\right), \tag{27}$$

with $c \simeq 2$. The above formula has been derived by assuming that the local exponent of the saturation scale

$$\lambda(Y) = \frac{d \ln(Q_{\rm s}(Y)/\Lambda)}{dY},$$

has the similar form as in the fixed coupling case

$$\lambda(Y) = c\,\alpha_{\rm s}\left(Q_{\rm s}^2(Y)\right).$$

By using these two formulae one can derive saturation scale in the running coupling case (27), see [17, 30].

10. Solution in (3+1) dimensions

10.1. Spatial distribution: impact parameter dependence

The phenomenon of saturation discussed so far has been based on the properties of the solution to the BK equation in $(1+1)$ dimensions. This approach completely ignores the spatial distribution of the probe-target system. The solution to $(1+1)$ dimensional BK equation is integrated over the impact parameter. This is a result of the fact that in $(1+1)$ dimensional BK equation we have assumed the infinite size of the target, and ignored any edge effects. One might expect, that the more realistic picture of saturation looks as follows: when the probe collides with the target, there is a dense system of partons in the limited region of the impact parameter space which has a finite radius. As one probes larger impact parameters, the density of partons becomes more and more dilute. When the energy grows, the radius of the dense, saturated system expands. This process is schematically drawn in Fig. 23. One expects that the impact parameter profile of the

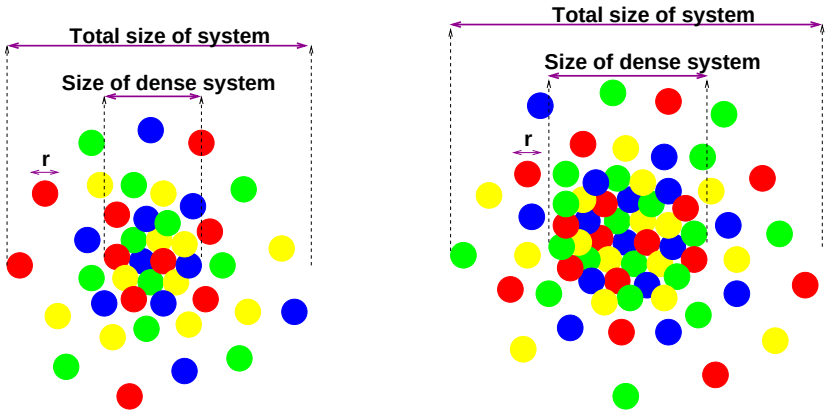

Fig. 23. Schematic picture of the impact parameter dependence of the parton density at high energies. Right plot: as energy increases the area of the saturated region, the *black disc*, increases.

scattering amplitude will have the behavior shown in Fig. 24. A question thus arises, whether BK equation can provide some information about the impact parameter profile of the amplitude, and whether it is consistent with the qualitative picture of saturation. Let us recall the BK equation with full dependence on all coordinates

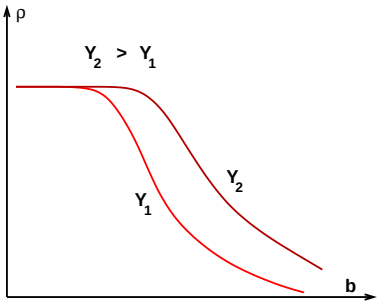

Fig. 24. Impact parameter dependence of the scattering amplitude for two different values of rapidity. As energy (rapidity) increases the radius of the saturated plateau also grows.

$$\frac{dN(\boldsymbol{b}_{01},\boldsymbol{x}_{01},Y)}{dY} = \bar{\alpha}_{\rm s}\int \frac{d^2\boldsymbol{x}_2\,\boldsymbol{x}_{01}^2}{\boldsymbol{x}_{20}^2\,\boldsymbol{x}_{12}^2}$$
$$\times\left[N\left(\boldsymbol{b}_{01}+\frac{\boldsymbol{x}_{12}}{2},\boldsymbol{x}_{20},Y\right)+N\left(\boldsymbol{b}_{01}-\frac{\boldsymbol{x}_{20}}{2},\boldsymbol{x}_{12},Y\right)-N(\boldsymbol{b}_{01},\boldsymbol{x}_{01},Y)\right.$$
$$\left.-N\left(\boldsymbol{b}_{01}+\frac{\boldsymbol{x}_{12}}{2},\boldsymbol{x}_{20},Y\right)\,N\left(\boldsymbol{b}_{01}-\frac{\boldsymbol{x}_{20}}{2},\boldsymbol{x}_{12},Y\right)\right]. \tag{28}$$

As already stated before, in general the problem is very difficult, even numerically since one has 4 degrees of freedom per dipole and one evolution variable, rapidity. Even though the integral measure does not depend on the positions of the dipoles, impact parameter dependence is generated through the couplings of b_{ij} to x_{ij} in the arguments of the functions N, see Eq. (28). To simplify the problem, and yet retain the information about the impact parameter dependence, we note that measure in the equation

$$\frac{d^2\boldsymbol{x}_2\,\boldsymbol{x}_{01}^2}{\boldsymbol{x}_{20}^2\,\boldsymbol{x}_{12}^2}\,,$$

is invariant under global rotations in transverse space

$$\boldsymbol{x}_0,\boldsymbol{x}_1,\boldsymbol{x}_2 \longrightarrow \mathcal{O}(\phi)\boldsymbol{x}_0,\mathcal{O}(\phi)\boldsymbol{x}_1,\mathcal{O}(\phi)\boldsymbol{x}_2\,,$$

see Fig. 25.

Thus we can assume that the position of the dipole is specified by three variables: its size r, impact parameter b and the relative orientation of the dipole with respect to the impact parameter axis (angle θ), see Fig. 25. The invariance with respect to global rotations is equivalent with a condition that the target is cylindrically symmetrical object. Thus the problem reduces to $(3+1)$ dimensions: $N(r,b,\theta,\phi;Y) \to N(r,b,\theta;Y)$. The BK equation with

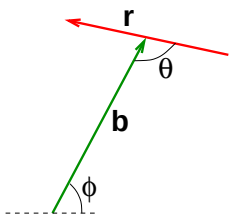

Fig. 25. Parametrization of dipole position.

the impact parameter dependence has been investigated numerically [32,33] see also [34]. Here we show some of the results taken from [32], where the initial distribution has been chosen to have a form of the Glauber–Mueller

$$N^{(0)}(r,b,\theta;Y=0)=1-\exp(-r^2S(b))\,, \tag{29}$$

where the impact parameter profile has been chosen to be Gaussian type

$$S(b)=\frac{1}{R_0^2}\exp\left(\frac{-b^2}{b_0^2}\right)\,. \tag{30}$$

10.2. Impact parameter dependence

In Fig. 26 we show resulting impact parameter dependence of the BK solution for different values of rapidity Y. For small values of impact parameter b the amplitude is large, and strong nonlinear effects are clearly visible. On the other hand, for large values of b one observes fast growth of the amplitude which is governed by the linear part of the equation. One can verify that the increase is exponential in rapidity as expected from BFKL equation. The region in impact parameter space where the amplitude is large, expands with rapidity. However, perhaps the most striking feature is the fact that the initial profile in impact parameter is not preserved even after small step in rapidity, $\Delta Y=0.1$. The exponential tail of the initial distribution has been immediately replaced by the power behavior $\sim 1/b^4$.

It is interesting to investigate the origin of these power tails. One can divide the region of integration into two parts: long and short range contributions by introducing a separating cutoff r_0 on the dipole size

$$\left[\overbrace{\int\Theta(r_0-|\boldsymbol{x}_2-\boldsymbol{b}|)}^{\text{short}}+\overbrace{\int\Theta(|\boldsymbol{x}_2-\boldsymbol{b}|-r_0)}^{\text{long}}\right]\frac{d^2\boldsymbol{x}_2(\boldsymbol{x}_0-\boldsymbol{x}_1)^2}{(\boldsymbol{x}_0-\boldsymbol{x}_2)^2(\boldsymbol{x}_1-\boldsymbol{x}_2)^2}$$
$$\times\left(N_{02}^{(0)}+N_{12}^{(0)}-N_{01}^{(0)}-N_{02}^{(0)}N_{12}^{(0)}\right)\,.$$

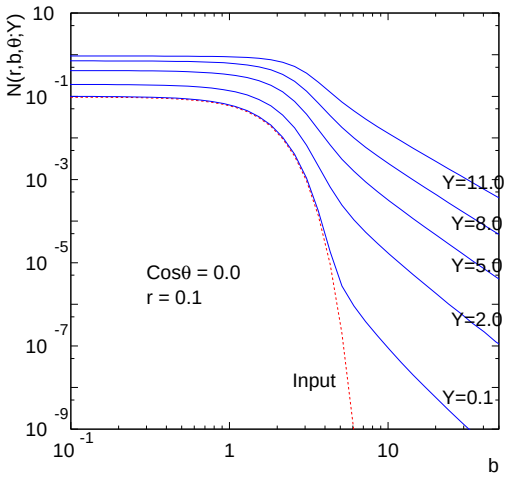

Fig. 26. Impact parameter dependence of the solution to the BK equation for increasing values of rapidity.

In Fig. 27 the profile in impact parameter space has been decomposed into short and long range contributions. One can see that the short range contribution is dominating the behavior at small values of b. There the exponential behavior is preserved since we have the factorization of initial profile $S(b)$ at small values of b. The long range contribution is dominating at large values of impact parameter b where it generates the power tail. Thus the $\sim 1/b^4$ behavior originates from the integration of the large dipole sizes and is a reflection of the asymptotic behavior of the integral kernel (see discussion in [35]).

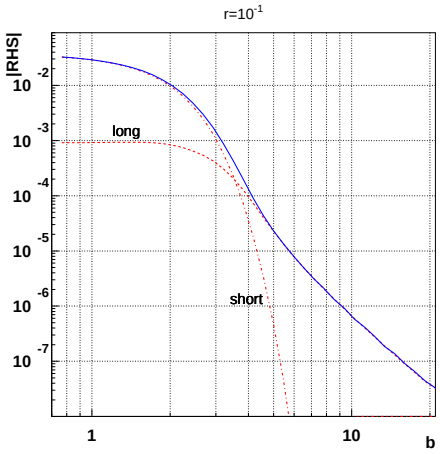

Fig. 27. The impact parameter dependence of the amplitude decomposed into the short and long range contributions after small evolution step in rapidity $\Delta Y = 0.1$.

10.3. Violation of Froissart bound

The presence of the power tail in impact parameter has profound consequences for the unitarity. Power decrease of the amplitude means that the interaction is long range. As already stated it is a direct consequence of the power-like form of the integral kernel

$$\frac{d^2\boldsymbol{x}_2\,\boldsymbol{x}_{01}^2}{\boldsymbol{x}_{20}^2\,\boldsymbol{x}_{12}^2} \simeq d^2\boldsymbol{x}_2\,\frac{r^2}{b^4}\,.$$

This type of fast expansion of the interaction system leads to the violation of the Froissart bound, as has been first observed in [35] (compare also a parallel discussion in [36]). It turns out that even though the amplitude is equal or less than 1 due to the nonlinearity of the equation, the dipole cross section increases fast with the decreasing x which violates Froissart bound

$$\sigma = \int d^2\boldsymbol{b}\,N(\boldsymbol{r},\boldsymbol{b};Y=\ln 1/x) \sim x^{-\lambda}\,.$$

This happens, because the kernel in BK equation is conformally invariant, with no mass scale which would cut off the long range contributions.

10.4. Dipole size dependence

The dipole size dependence in the case of impact parameter dependent BK equation is shown in Fig. 28 where the value for impact parameter has been chosen to correspond to a central collision. For small and moderate values of r it has qualitatively the same behavior as previously, amplitude is vanishing as r tends to 0 and extending to lower values of r as rapidity grows. It also saturates to 1 for moderate values of r. However, at large values of dipole size the situation is dramatically different, here the amplitude drops down again. The reason is that now there is a dimension in impact parameter which characterizes the size of the target. As the dipole grows, at some point it will completely miss the target and amplitude will become zero again. This is quite different from the previous case (without impact parameter) where the amplitude was always saturated since there was an infinite target. It is also interesting to study solution at different values of b. In Fig. 29 we present the dipole size dependence of the amplitude for larger value of b which corresponds to a peripheral collision of the dipole with the target. In that case we see that the amplitude peaks for values of the dipole size which are twice as large as the impact parameter. This is expected since it reflects the properties of the integral kernel in the BK equation. The solution in the b-dependent case has also some other interesting properties. For values of dipole size which are small when compared with the impact

parameter $r \ll b$, the amplitude depends only on one combined variable r^2/b^4. This dependence on one variable, *an-harmonic ratio* , is the result of the conformal symmetry, see for example [11].

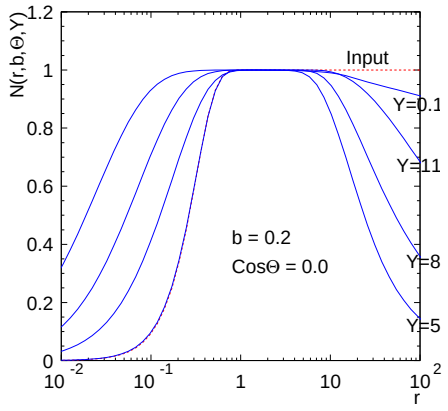

Fig. 28. Solution of the impact parameter dependent BK equation with fixed orientation and position of the dipole for various values of rapidity $Y = 0.1, 5, 8, 11$.

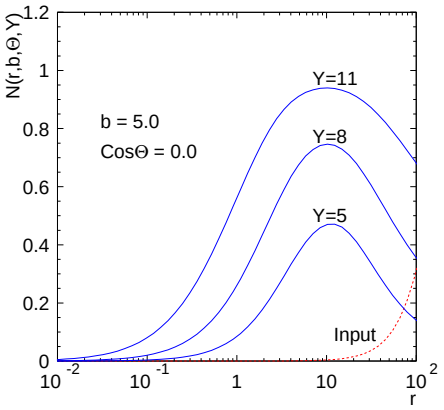

Fig. 29. The same as Fig. 28 but for large value of impact parameter $b = 5$.

10.5. Saturation scale with b dependence

One can also extract the saturation scale from the solution to BK equation in $(3+1)$ dimensions. In [32] a following prescription has been used

$$\langle N(r = 1/Q_{\rm s}, b, \theta; Y)\rangle_\theta = \kappa, \qquad \kappa \sim 0.5\,. \tag{31}$$

From Fig. 28 we see that Eq. (31) possesses two solutions

$$\frac{1}{Q_{\rm s}(b,Y)} < r < R_{\rm H}(b,Y)\,.$$

The lower bound $Q_{\rm s}(b,Y)$ is the impact parameter dependent saturation scale, which has been plotted in Fig. 30. We see that the saturation scale has strong dependence on b, it is largest at small values of impact parameter and then decreases for large values of impact parameter. The physical picture is that while the impact parameter is increased, one moves from a strongly saturated regime to a more dilute one. The tail of the saturation scale is again power like $\sim 1/b^2$ which is to be expected from the properties of the integral kernel. We see that this behavior is quite different from the one that would be anticipated from initial conditions (compare dashed lines). The saturation scale has the following behavior

$$Q_{\rm s}^2(b,Y) \simeq g(b)\,\exp(\bar{\alpha}_{\rm s} 2\lambda_{\rm s} Y), \qquad \lambda_{\rm s} \simeq 2\,,$$

where function $g(b)$ is exponentially falling for small values of b and has a power like behavior at large values of impact parameter.

The second solution $R(b,Y)$ is new compared to the b-independent case, and it just reflects the fact the there is an additional scale present, the finite size of the target and that we no longer have an infinitely large target.

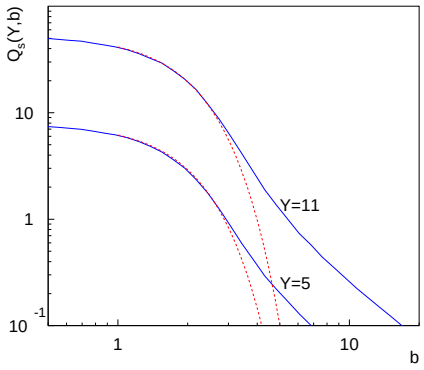

Fig. 30. Impact parameter profile of the saturation scale for two various rapidities $Y = 5$ and $Y = 11$. Solid lines are the result of the calculation of full BK equation. Dashed lines correspond to the exponential behavior of the saturation scale that was expected from initial conditions.

11. Conclusions and outlook. Beyond BK equation

We have described basic properties of the BK equation which is a non-linear evolution equation suitable for description of partonic systems at high density. We showed that the solution to this equation has a property of geometrical scaling, with the characteristic saturation scale. The nice property of this equation is the suppression of the infrared diffusion and independence of the regularization for the running coupling. The impact parameter dependence of this equation leads to the violation of the Froissart bound despite the fact that the amplitude is bounded from above. This is a consequence of purely perturbative approach and lack of long distance effects such as confinement in the BK equation.

However, BK equation has been derived by using strong assumptions about lack of correlations in the system and it is thus an equation in mean field approximation. It is not clear to what extent the BK equation is a good approximation to the full Balitsky–JIMWLK equations. In numerical studies of the dipole scattering by Salam [37] it has been shown that the fluctuations are very important and lead to a very different result as compared with the mean field approach. A lot of theoretical effort has been recently devoted to study the role of correlations: in [38] a more quantitative study of the fluctuations has been proposed, in [39] a new equation for the generating functional was postulated which takes into account correlations in the nuclei; in [40] a BK equation with two absorptive boundaries has been studied; in [41] a numerical study of the full JIMWLK equation has been performed for the first time; in [42] an analytical study of the Balitsky hierarchy restricted to the dipole operators and in [43] the role of the discreetness of the gluon system and connection to the statistical physics have been discussed. We expect that this line of research will be continued in the near future and we will be able to understand the fascinating and complex theory of strong interactions even better.

This research is supported by the U.S. Department of Energy, Contract No. DE-AC02-98CH10886.

REFERENCES

[1] L.N. Lipatov, *Sov. J. Nucl. Phys.* **23**, 338 (1976); E.A. Kuraev, L.N. Lipatov, V.S. Fadin, *Sov. Phys. JETP* **45**, 199 (1977); I.I. Balitsky, L.N. Lipatov, *Sov. J. Nucl. Phys.* **28**, 338 (1978).

[2] L.V. Gribov, E.M. Levin, M.G. Ryskin, *Phys. Rep.* **100**, 1 (1983).

[3] M. Froissart, *Phys. Rev.* **123**, 1053 (1961); A. Martin, *Phys. Rev.* **129**, 1432 (1963).

[4] L. McLerran, R. Venugopalan, *Phys. Rev.* **D49**, 2233 (1994); *Phys. Rev.* **D49**, 3352 (1994); *Phys. Rev.* **D50**, 2225 (1994); J. Jalilian-Marian, A. Kovner, L. McLerran, H. Weigert, *Phys. Rev.* **D55**, 5414 (1997); R. Venugopalan, *Acta Phys. Pol. B* **30**, 3731 (1999); E. Iancu, A. Leonidov, L. McLerran, *Nucl. Phys.* **A692**, 583 (2001); E. Ferreiro, E. Iancu, A. Leonidov, L. McLerran, *Nucl. Phys.* **A701**, 489 (2002); E. Iancu, R. Venugopalan, `hep-ph/0303204`.

[5] J. Jalilian-Marian, A. Kovner, A. Leonidov, H. Weigert, *Nucl. Phys.* **B504**, 415 (1997); *Phys. Rev.* **D59**, 014014 (1999). J. Jalilian-Marian, A. Kovner, H. Weigert, *Phys. Rev.* **D59**, 014015 (1999).

[6] H. Weigert, *Nucl. Phys.* **A703**, 823 (2002).

[7] I.I. Balitsky, *Nucl. Phys.* **B463**, 99 (1996); I.I. Balitsky, *Phys. Rev. Lett.* **81**, 2024 (1998); *Phys. Rev.* **D60**, 014020 (1999).

[8] Yu.V. Kovchegov, *Phys. Rev.* **D60**, 034008 (1999).

[9] A.H. Mueller, *Nucl. Phys.* **B415**, 373 (1994).

[10] V.N. Gribov, L.N. Lipatov, *Sov. J. Nucl. Phys.* **15**, 438 (1972); Yu.L. Dokshitzer, *Sov. Phys. JETP* **46**, 641 (1977); G. Altarelli, G. Parisi, *Nucl. Phys.* **B126**, 298 (1977).

[11] L.N. Lipatov, *Sov. Phys. JETP* **63**, 904 (1986).

[12] S. Munier, A.M. Stasto, A.H. Mueller, *Nucl. Phys.* **B603**, 427 (2001).

[13] K. Golec–Biernat, M. Wüsthoff, *Phys. Rev.* **D59**, 014017 (1999); *Phys. Rev.* **D60**, 114023 (1999); *Eur. Phys. J.* **C20**, 313 (2001).

[14] M.A. Braun, *Eur. Phys. J.* **C16**, 337 (2000).

[15] N. Armesto, M.A. Braun, *Eur. Phys. J.* **C20**, 517 (2001); J.L. Albacete, N. Armesto, A. Kovner, C.A. Salgado, U.A. Wiedemann, *Phys. Rev. Lett.* **92**, 082001 (2004).

[16] M. Lublinsky, E. Gotsman, E. Levin, U. Maor, *Nucl. Phys.* **A696**, 851 (2001); M. Lublinsky, *Eur. Phys. J.* **C21**, 513 (2001); E. Gotsman, E. Levin, M. Lublinsky, U. Maor, *Eur. Phys. J.* **C27**, 411 (2003).

[17] K. Golec-Biernat, L. Motyka, A.M. Staśto, *Phys. Rev.* **D65**, 074037 (2002).

[18] E. Levin, K. Tuchin, *Nucl. Phys.* **B573**, 833 (2000); *Nucl. Phys.* **A691**, 779 (2001); *Nucl. Phys.* **A693**, 787 (2001).

[19] S. Munier, R. Peschanski *Phys. Rev. Lett.* **91**, 232001 (2003); *Phys. Rev.* **D69**, 034008 (2004); `hep-ph/0401215`.

[20] J. Bartels, V. Fadin, L.N. Lipatov, *Nucl. Phys.* **B696**, 255 (2004).

[21] A.H. Mueller, D.N. Triantafyllopoulos, *Nucl. Phys.* **B640**, 331 (2002).

[22] A. Staśto, K. Golec-Biernat, J. Kwieciński, *Phys. Rev. Lett.* **86**, 596 (2001).

[23] N. Armesto, C.A. Salgado, U.A. Wiedemann, `hep-ph/0407018`; A. Freund, K. Rummukainen, H. Weigert, A. Schafer, *Phys. Rev. Lett.* **90**, 222002 (2003).

[24] R.A. Fisher, *Ann. Eugenics* **7**, 355 (1937); A. Kolmogorov, I. Petrovsky, N. Piscounov, *Moscow Univ. Bull. Math.* **A1**, 1 (1937).

[25] W. van Saarlos, *Phys. Rep.* **386**, 29 (2003).

[26] V.S. Fadin, M.I. Kotsky, R. Fiore, *Phys. Lett.* **B359**, 181 (1995); V.S. Fadin, M.I. Kotsky, L.N. Lipatov, BUDKERINP-96-92, hep-ph/9704267; V.S. Fadin, R. Fiore, A. Flachi, M.I. Kotsky, *Phys. Lett.* **B422**, 287 (1998); V.S. Fadin, L.N. Lipatov, *Phys. Lett.* **B429**, 127 (1998); G. Camici, M. Ciafaloni, *Phys. Lett.* **B386**, 341 (1996); *Phys. Lett.* **B412**, 396 (1997), Erratum *Phys. Lett.* **B417**, 390 (1997); *Phys. Lett.* **B430**, 349 (1998).

[27] M.A. Braun, *Phys. Lett.* **B576**, 115 (2003).

[28] J.L. Albacete, N. Armesto, J.G. Milhano, C.A. Salgado, U.A. Wiedemann, hep-ph/0408216.

[29] D.D. Dietrich, hep-ph/0411192.

[30] E. Iancu, K. Itakura, L. McLerran, *Nucl. Phys.* **A708**, 327 (2002).

[31] D.N. Triantafyllopoulos http://arxiv.org/find/hep-ph/1/au:+Triantafyllopoulos_D/0/1/0/all/0/1, *Nucl. Phys.* **B648**, 293 (2003).

[32] K. Golec-Biernat, A.M. Staśto, *Nucl. Phys.* **B668**, 345 (2003).

[33] E. Gotsman, M. Kozlov, E. Levin, U. Maor, E. Naftali, *Nucl. Phys.* **A742**, 55 (2004).

[34] T. Ikeda, L. McLerran, hep-ph/0410345.

[35] A. Kovner, U.A. Wiedemann, *Phys. Rev.* **D66**, 051502 (2002); *Phys. Rev.* **D66**, 034031 (2002); *Phys. Lett.* **B551**, 311 (2003).

[36] E. Ferreiro, E. Iancu, K. Itakura, L. McLerran, *Nucl. Phys.* **A710**, 373 (2002).

[37] G.P Salam, *Nucl. Phys.* **B449**, 589 (1995); *Nucl. Phys.* **B461**, 512 (1996); A.H. Mueller, G.P. Salam, *Nucl. Phys.* **B475**, 293 (1996).

[38] E. Iancu, A.H. Mueller, *Nucl. Phys.* **A730**, 494 (2004).

[39] E. Levin, M. Lublinsky, *Nucl. Phys.* **B370**, 191 (2004); hep-ph/0411121 .

[40] A.H. Mueller, A. Shoshi, *Nucl. Phys.* **B692**, 175 (2004).

[41] K. Rummukainen, H. Weigert, *Nucl. Phys.* **B739**, 183 (2004).

[42] R.A. Janik, R. Peschanski, hep-ph/0407007; R.A. Janik, hep-ph/0409256.

[43] E. Iancu, A.H. Mueller, S. Munier, hep-ph/0410018.